Nanoscale Optical Electrometer

A. N. Vamivakas,[1] Y. Zhao,[1,2] S. Fält,[3] A. Badolato,[4] J. M. Taylor,[5,6] and M. Atatüre[1]

[1]*Cavendish Laboratory, University of Cambridge, JJ Thomson Avenue, Cambridge CB3 0HE, United Kingdom*
[2]*Physikalisches Institut, Ruprecht-Karls-Universität Heidelberg, Philosophenweg 12, 69120 Heidelberg, Germany*
[3]*Sol Voltaics AB, Scheelevägen 17, Ideon Science Park, 223 70 Lund, Sweden*
[4]*Department of Physics and Astronomy, University of Rochester, Rochester, New York 14627, USA*
[5]*Department of Physics, Massachusetts Institute of Technology, 77 Massachusetts Ave, Cambridge, Massachusetts 02139, USA*
[6]*Joint Quantum Institute/National Institute of Standards of Technology, 100 Bureau Drive MS 8423, Gaithersburg, Maryland 20899, USA*

(Received 26 May 2011; published 11 October 2011)

We propose and demonstrate an all-optical approach to single-electron sensing using the optical transitions of a semiconductor quantum dot. The measured electric-field sensitivity of 5 $(\mathrm{V/m})/\sqrt{\mathrm{Hz}}$ corresponds to detecting a single electron located 5 μm from the quantum dot—nearly 10 times greater than the diffraction limited spot size of the excitation laser—in 1 s. The quantum-dot-based electrometer is more sensitive than other devices operating at a temperature of 4.2 K or higher and further offers suppressed backaction on the measured system.

DOI: 10.1103/PhysRevLett.107.166802 PACS numbers: 85.35.Be, 06.20.−f, 07.07.Df, 42.50.−p

Self-assembled semiconductor quantum dots (QDs) show remarkable optical and spin coherence properties, which have led to a concerted research effort examining their potential as a quantum bit for quantum information science [1–6]. We present an alternative application for such devices, exploiting recent achievements of charge occupation control and the spectral tunability of the optical emission of QDs by electric fields [7,8] to demonstrate high-sensitivity electric-field measurement. In contrast to existing nanometer-scale electric-field sensors, such as single-electron transistors [9–12] and mechanical resonators [13,14], our approach relies on homodyning light resonantly Rayleigh scattered from a QD transition with the excitation laser and phase-sensitive lock-in detection. The homodyne signal, in combination with the lock-in electronics, offers static and transient field detection ability, high bandwidth operation, and near-unity quantum efficiency, where each laser photon that interacts with the quantum dot contributes to the sensor signal.

The electric-field dependence of QDs originates from an inherent displacement of the confined electron and hole wave functions. The displacement (~ 0.5 nm) generates a nonzero permanent exciton dipole moment [15] which leads to a linear Stark shift $\sim \alpha \boldsymbol{n} \cdot \boldsymbol{E}$ of the transition under an applied electric field $\boldsymbol{E}$ (α is the permanent dipole moment, and $\boldsymbol{n}$ is the QD growth direction). Figure 1(a) presents a schematic of our QD sensor concept. A single electron generates an electric field at the location of the QD that is monitored via resonant light scattering. An example of the response to a single, proximal electron is shown in Fig. 1(b). The device consists of 2 vertically stacked InAs QDs embedded in a Schottky diode separated by 13 nm [16]. In this structure, asymmetric exchange coupling of the charges allowed for the measurement of the spin of a resident electron in one QD by the optical transitions of the other QD [17]. In the regime where there is no tunnel coupling, the neighboring QD optical transitions are not spin-sensitive but are responsive to electric charge. The top panel of Fig. 1(b) shows the absorption resonance of QD2 when QD1 is uncharged, and the bottom panel shows the QD2 absorption resonance when a single electron is loaded into QD1 (but not QD2). The spectral shift (~ 18 times the transition linewidth) is a manifestation of single-electron charge sensing [18] arising from the linear Stark effect. To quantify the linear Stark effect, the absorption resonance of a single QD, in a second device [16], is monitored as a function of an externally applied electric field in Fig. 1(c). The absorption resonance slope determines a linear Stark shift coefficient α of 0.028 $\mathrm{MHz\,m/V}$ characterizing this QD transition's electric-field response.

Building off the previous, in this Letter, we demonstrate theoretical and operational electric-field sensitivity limits of a single QD device. Our approach relies on the interference of the excitation laser with the QD transition forward and backward scattered light and modulation spectroscopy, i.e., differential transmission (DT) and reflection (DR) [19,20]. Application of a *sublinewidth* gate voltage modulation across the device and a lock-in amplifier-based detection of the absorptive DT (dispersive DR) signals isolates the local static (transient) electric-field component in the DT (DR) signal. Figure 2 schematically illustrates the sensor operating principle. The sublinewidth modulation allows the excitation laser to sample, in each lock-in period, symmetric (antisymmetric) points in the absorptive DT (dispersive DR) line shape. This coordinated sampling and the 180° phase shift imparted to voltage values reported by the phase-sensitive lock-in in each half-period results in a device sensitive only to static (transient) electric fields.

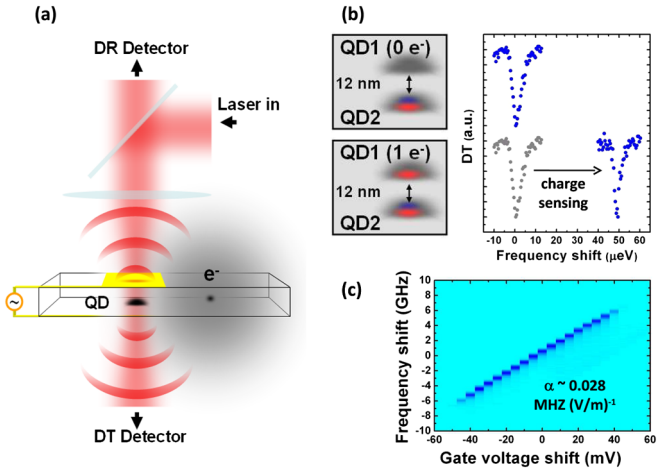

FIG. 1 (color online). (a) Illustration of the experimental apparatus. Laser light is focused onto the sample and is homodyned with Rayleigh scattered light in the forward (backward) direction for dc (ac) sensing. (b) Single electric charge sensing with a vertically stacked quantum dot molecule. The top left panel is an illustration of the excited state configuration with 1 electron and 1 hole in the bottom quantum dot and no charge in the top quantum dot. The bottom left panel is an illustration of the excited state configuration with 1 electron and 1 hole in the bottom quantum dot and 1 electron in the top quantum dot. The right panel is the absorption spectrum corresponding to this excited state. (c) DT spectroscopy of the QD transition. The laser power equals the saturation power, and the QD gate voltage is modulated by a square wave with peak-to-peak amplitude of 100 mV.

Our detection approach is limited fundamentally by the optical theorem which relates the maximum amount of resonance fluorescence to the transition's radiative lifetime. It achieves unit quantum efficiency since every photon scattered leads to DT or DR signal. The rate of photons incident on the QD is given by the rate of photons incident on the detector in the absence of the QD scaled by $p = \frac{4}{9}n^2(\mathrm{NA})^2$, with a Rabi frequency

$$\Omega = \sqrt{\frac{P}{\hbar\omega}\frac{\gamma_{\mathrm{sp}}}{p}}, \tag{1}$$

where n is the refractive index, NA the lensing system numerical aperture, P the laser power, ω the laser frequency, and γ_{sp} the spontaneous emission rate. Assuming a Lorentzian line shape for the underlying transition with a linewidth Γ, the rate of photons incident on the detector is

$$\dot{n} = \frac{\Omega^2}{\gamma_{\mathrm{sp}}}\left(p - \frac{2\gamma_{\mathrm{sp}}\Gamma}{\Delta^2 + \Gamma^2 + 4\Omega^2\Gamma/\gamma_{\mathrm{sp}}}\right), \tag{2}$$

where Δ is the electric-field-dependent spectral detuning of the laser from the QD transition. The corresponding shot noise is $\sqrt{\dot{n}t}$, so the signal-to-noise improves by the square root of averaging time, leading to our electric-field sensitivity of

$$\eta = \varepsilon^{-1/2}\alpha^{-1}\frac{\sqrt{\dot{n}}}{\partial\dot{n}/\partial\Delta}. \tag{3}$$

This is optimal for $\Delta = \Gamma/\sqrt{2}$ and $\Omega = \sqrt{\gamma_{\mathrm{sp}}\Gamma/8}$, giving

$$\eta_0 = \varepsilon^{-1/2}\alpha^{-1}\frac{4\Gamma^{3/2}\sqrt{p}}{\gamma_{\mathrm{sp}}}. \tag{4}$$

For our experimental parameters, the best attainable sensitivity is $\sim 0.5\ (\mathrm{V/m})/\sqrt{\mathrm{Hz}}$, which corresponds to detecting a single electron at a distance of 16 μm in 1 s. Since the local electric field is measured via light scattering, the sensor bandwidth is limited fundamentally by the exciton transition spontaneous emission rate γ_{sp} (~ 1 GHz).

We next characterize the QD device as a static electric-field sensor. A trace of the mean DT signal is presented in Fig. 3(a) when the transition is driven slightly above saturation and the square wave modulation peak-to-peak voltage amplitude is 1 mV, corresponding to 0.14 GHz on the abscissa. Evident in Fig. 3(a) is the mean DT signal variation around the resonance—the dc sensor operating point (orange diamond)—as compared to frequency shifts greater than ± 0.25 GHz. Figure 3(b) displays the standard deviation of the time traces, recorded at the 3 spectral locations identified in Fig. 3(a), as the measurement time constant is increased. Measurements performed away from the resonance (0.75 GHz laser detuning) in Fig. 3(b) display that the resulting noise (open blue circles) reduces to the square root of the averaging time (black line in the inset), as expected from white noise within our measurement bandwidth. The same behavior is observed when the laser is detuned 0.25 GHz from the resonance (open red squares), where, as can be seen in Fig. 3(a), the static electric-field dependence is expected to be suppressed while still detecting DT signal. However, on the resonance, the noise behavior deviates from the square-root dependence on measurement time, indicating a departure from white noise towards $1/f$-type noise. This behavior, arising from charge dynamics in the QD environment, is interesting and will be further studied elsewhere. To quantify the dc field sensitivity, we follow Eq. (2) and divide the measured system noise, at 0.75 GHz detuning, by the slope of the mean DT signal at the sensor operating point [orange diamond in Fig. 3(a)]. Figure 3(c) presents the laser power dependence of the electric-field sensitivity, η, as predicted by Eqs. (2) and (3). In this plot, larger values of the sensitivity η correspond to an operation point that requires larger external fields to generate a sensor response, i.e., poorer performance. We find the sensor is most sensitive at 1.5 nW excitation laser power, which corresponds to saturation ($\Omega \approx \Gamma$) marking the optimum operating excitation laser power for the sensor. A sensitivity of 5 $(\mathrm{V/m})/\sqrt{\mathrm{Hz}}$ is obtained across a 100 MHz window around the operating point for the data in Fig. 3(a). This level of electric-field sensitivity corresponds to the experimental ability to distinguish the electric field generated by a single electron

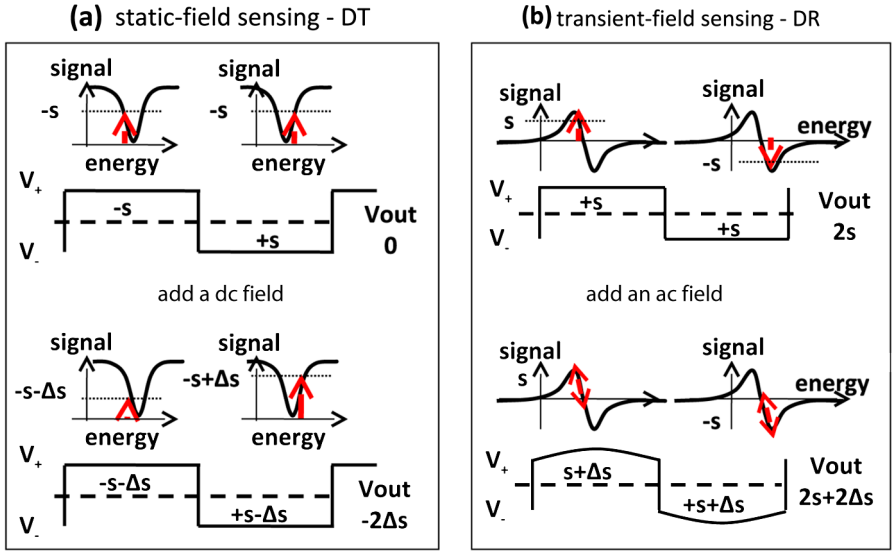

FIG. 2 (color online). (a) Description of static electric-field (dc) sensing. A small sublinewidth voltage modulation is applied to the device to enable lock-in detection. The top panel illustrates 1 cycle of the lock-in detector when the laser (vertical red arrow) is tuned to the point of highest slope for the Lorentzian response, reporting a signal level $-s$. The lock-in output in this case is 0. The lower panel is 1 cycle of the lock-in detector, but here the laser is detuned from the highest slope point due to the presence of an applied electric field. The lock-in reports a nonzero voltage that reveals the magnitude and polarity of the applied electric field. (b) Description of transient electric-field (ac) sensing. The modulation frequency determines the measured frequency component of the local oscillating electric field. The top panel illustrates 1 cycle of the lock-in detector when the laser (vertical red arrow) is tuned to a point such that the lock-in reports a signal level $-2s$. The lower panel is 1 cycle of the lock-in detector in the presence of an applied transient electric field oscillating at the lock-in frequency. The lock-in reports an additional voltage that reveals the magnitude of this oscillating field.

located ~ 5 μm away from the device in 1 s, well outside the optically accessed volume in our current device. This sensitivity is not fundamentally limited and depends strongly on the Stark coefficient α, as is evident in Eq. (4). An improved sensitivity of 0.95 $(\mathrm{V/m})/\sqrt{\mathrm{Hz}}$ was obtained on another QD with a larger Stark coefficient (not shown).

To characterize the QD transient (ac) electric-field sensing performance, we use the DR signal. Figure 4(a)

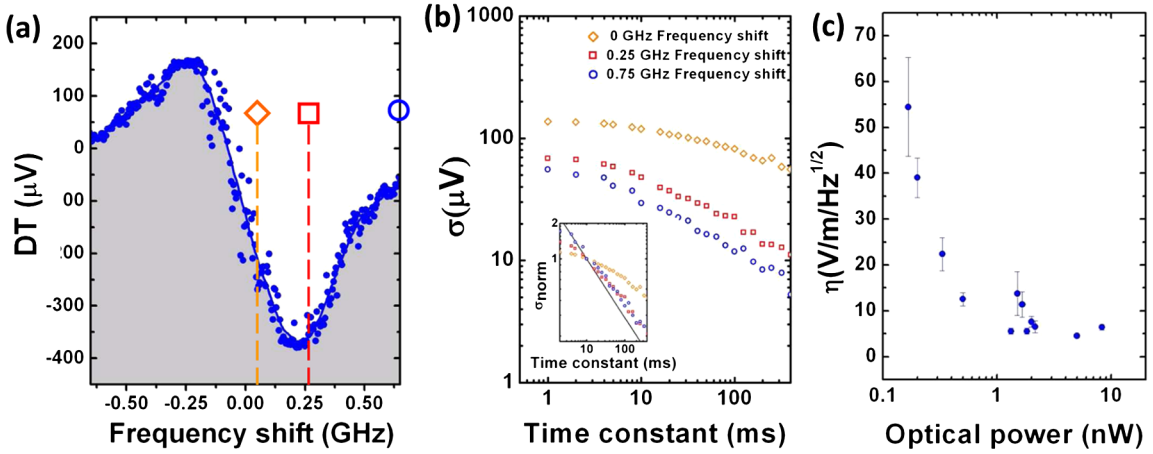

FIG. 3 (color online). (a) Absorption spectrum of a single quantum dot (DT). Each data point is recorded for 8 s with 1-ms time resolution. (b) A log-log plot of the variation of measurement noise, quantified by the standard deviation, with measurement time constant. Each data point is determined by subdividing the measured time trace into a collection of equal size time bins, finding the mean of each time bin, and then finding the standard deviation of the collection of means. The open orange diamonds correspond to 0 frequency shift in (a), the open red squares to 0.25 frequency shift, and the open blue circles to 0.75 frequency shift. At the dc sensor operating point—0 frequency shift—the noise magnitude is largest. Inset: same noise data, but all curves are normalized to 1 at 10 ms time constant. The black line plots the inverse square root of the measurement time constant. For spectral locations away from the dc electrometer operating point [0 frequency shift in (a)], the noise exhibits the expected time constant dependence. When the laser is at the electrometer operating spectral region, the measured noise is colored as indicated by the departure of the data from the black line. (c) The laser power dependence of the measured sensitivity when the laser is resonant with the QD transition.

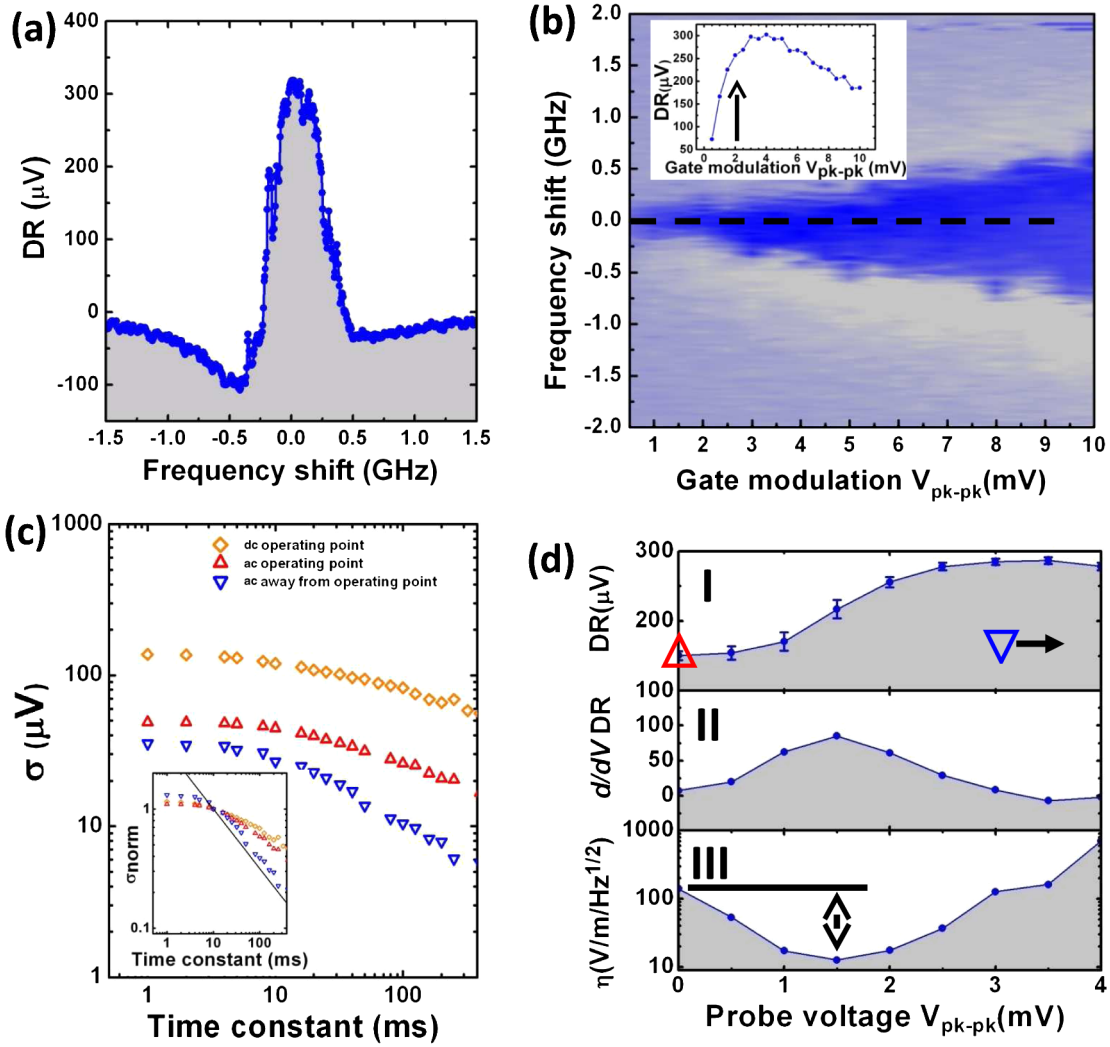

FIG. 4 (color online). (a) A DR spectrum of a single QD. Each data point is recorded for 8 s with 1-ms time resolution. (b) DR spectroscopy of the QD transition as the square wave modulation peak-to-peak voltage is varied. Inset: DR signal along the black dashed line. The vertical arrow identifies the square wave modulation peak-to-peak voltage of 2 mV used for the data presented in (c), (d). (c) A log-log plot of the variation of measurement noise, quantified by the standard deviation, with measurement time constant. The open orange diamonds correspond to the dc electrometer operating point presented in Fig. 3(a). The point-up red (point-down blue) triangles correspond to ac noise when the ac electrometer is characterized at (away) from its operating point. Inset: normalized as in Fig. 3(b). The black line plots the inverse square root of the measurement time constant. (d) Panel I: DR signal when the laser power is slightly above saturation, the peak-to-peak amplitude of the square wave modulation is 2 mV, and the amplitude of an additional sine wave applied to the QD gate is varied. Each point is determined from the mean of 8 s worth of data acquired with 0.5-ms time bins. The error bars correspond to 1 standard deviation for 1 s of averaging time. Panel II: numerical derivative of panel I. Panel III: sine wave peak-to-peak voltage amplitude dependence of the ac sensitivity. To calculate the sensitivity, the standard deviation of each time trace is evaluated by subdividing the full time trace into 80 ms bins, finding the average of each bin, and then evaluating the standard deviation of this collection of means.

displays the measured DR signal with a small, subline-width voltage modulation. The deviation of the line shape from the second derivative of an ideal Lorentzian originates from the phase between the laser and the Rayleigh scattered light, as determined by the distance between the QD and the top surface of the sample. Figure 4(b) presents fixed gate voltage DR spectroscopy of the QD transition for a range of voltage modulation amplitudes ($V_{\text{pk-pk}}$). We identify the operating modulation peak-to-peak amplitude by analyzing the DR line cut (inset) in Fig. 4(b) (solid vertical black line). The arrow indicates the 2-mV operating amplitude, which provides the gradient sensitive to an oscillatory field at the lock-in frequency. Since the sensor is only responsive to a transient electric field at the lock-in frequency, it is necessary to repeat the measurement as a function of lock-in frequency to build the full transient field spectrum. In Fig. 4(c), similar to the analysis presented in Fig. 3(b), the noise follows the square-root

dependence on measurement time when the voltage modulation is outside the electric-field sensitive high-gradient regime (point-down blue open triangles). The noise behavior also exhibits a deviation in the field sensitive region (point-up open red triangles) similar to the dc sensor (open orange diamonds). This is a direct outcome of suppressed (by a factor of 3) but not fully rejected low frequency charge dynamics discussed above. One advantage of our ability to simultaneously record the DR and DT signals is that residual coupling of low frequency signals can be subtracted from the DR signal, electronically allowing further noise rejection for the ac sensor.

Determination of the ac electrometer's sensitivity η is accomplished by exposing our device to an external (weak) sinusoidal field for a range of amplitudes and frequencies. The laser is tuned to resonance and fixed to saturation power. Panel I of Fig. 4(d) plots the mean DR signal, as the modulation amplitude of the additional field is varied (the additional field frequency is equal to the lock-in frequency; to measure a different transient field frequency, the lock-in frequency needs to be changed). The mean DR signal and its derivative (panel II) are used to calculate the sensitivity in panel III in accordance with Eq. (3) using the noise level obtained in the absence of residual dc coupling. The measured sensitivity η, 140 $(\mathrm{V/m})/\sqrt{\mathrm{Hz}}$, depends on the modulation amplitude of the sinusoidal voltage and it reduces to 14 $(\mathrm{V/m})/\sqrt{\mathrm{Hz}}$ for an input sinusoidal field amplitude of 1.5 mV due to the nonlinear gradient of this transition response [panel III of Fig. 4(d)]. A wavelength-optimized distance between the QD and the top surface should provide a more linear response, whereby the sensitivity would be input-amplitude independent. For our system, we find a sensitivity of 140 $(\mathrm{V/m})/\sqrt{\mathrm{Hz}}$ for an electric field oscillating at 1.908 kHz with a resolution of 10 Hz determined solely by the lock-in electronics.

The measured sensitivity of our device, comparable to the single-electron transistor, corresponds to detecting a single electron at a distance of 5 μm from the QD in 1 s. The ability to detect electron dynamics occurring outside of the optically probed volume enables our device to be used to monitor the charge occupancy of target structures, such as lateral QDs or Cooper pairs in a superconducting qubit, without altering their operational conditions, i.e., without perturbation from the excitation laser. Also, the QD detection ability does not depend on the overall electric field through a volume, as it might in a capacitive detector, but only on the field at the location of the QD confined to 20 nm. Thus, our device is best applied for situations with high electric-field densities but low total electrical energy. Further, the main back action of our device on the electron being detected originates only from the residual dipolar field due to the strongly confined charge neutral exciton; therefore, our system is considerably (already around 1000-fold at a distance of 1 μm) less invasive than devices relying on charge transport alone. Conditional on reasonable sample structure technical improvements and improved light extraction efficiency [21], our system has the potential to surpass the current state-of-the-art single-electron-transistor electrometer. Finally, our system can also operate as a magnetometer [22–25] via the linear Zeeman shift of 30 GHz/T for the QD transition, yielding a sensitivity of $\sim 5 \times 10^{-6}$ $\mathrm{T}/\sqrt{\mathrm{Hz}}$.

This work was supported by grants and funds from the University of Cambridge, EPSRC Grant No. EP/G000883/1, and the Cambridge-MIT Exchange Grant No. P019. Y. Z. is supported by the A. v. Humboldt Foundation and LGFG. The authors thank Charles Smith and Naomi Nickerson for useful discussions and technical assistance.

[1] A. Imamoglu *et al.*, Phys. Rev. Lett. **83**, 4204 (1999).
[2] P. Michler *et al.*, Science **290**, 2282 (2000).
[3] J. Kim, O. Benson, H. Kan, and Y. Yamamoto, Nature (London) **397**, 500 (1999).
[4] R. M. Stevenson *et al.*, Nature (London) **439**, 179 (2006).
[5] R. Hanson and D. D. Awschalom, Nature (London) **453**, 1043 (2008).
[6] F. Henneberger and O. Benson, *Semiconductor Quantum Bits* (Pan Stanford Publishing, Singapore, 2009).
[7] R. J. Warburton *et al.*, Nature (London) **405**, 926 (2000).
[8] A. Faraon *et al.*, Phys. Rev. Lett. **104**, 047402 (2010).
[9] M. Field *et al.*, Phys. Rev. Lett. **70**, 1311 (1993).
[10] D. J. Mar, R. M. Westervelt, and P. F. Hopkins, Appl. Phys. Lett. **64**, 631 (1994).
[11] R. J. Schoelkopf *et al.*, Science **280**, 1238 (1998).
[12] H. Brenning *et al.*, J. Appl. Phys. **100**, 114321 (2006).
[13] A. N. Cleland and M. L. Roukes, Nature (London) **392**, 160 (1998).
[14] J. Lee, Y. Zhu, and A. A. Seshia, J. Micromech. Microeng. **18**, 025033 (2008).
[15] R. J. Warburton *et al.*, Phys. Rev. B **65**, 113303 (2002).
[16] See Supplemental Material at http://link.aps.org/supplemental/10.1103/PhysRevLett.107.166802 for a description of the sample structures used in this work.
[17] A. N. Vamivakas *et al.*, Nature (London) **467**, 297 (2010).
[18] S. Fält *et al.*, Phys. Rev. Lett. **100**, 106401 (2008).
[19] K. Karrai and R. J. Warburton, Superlattices Microstruct. **33**, 311 (2003).
[20] B. Alén *et al.*, Appl. Phys. Lett. **89**, 123124 (2006).
[21] A. N. Vamivakas *et al.*, Nano Lett. **7**, 2892 (2007).
[22] J. M. Taylor *et al.*, Nature Phys. **4**, 810 (2008).
[23] C. L. Degen, Appl. Phys. Lett.**92**, 243111 (2008).
[24] J. R. Maze *et al.*, Nature (London) **455**, 644 (2008).
[25] G. Balasubramanian *et al.*, Nature (London) **455**, 648 (2008).